Supplementary Information

Enhanced the photothermal catalytic performance and stability of Ni–MOx−Al_2O_3 (M = Ce, Pr, Y) for DRM: the role of rare earth element

Jiming Wang[a], Min Ji[*a] and Min Wang[*a]

[a] School of Chemistry, Dalian University of Technology, Dalian 116024, PR China

[*] Corresponding author. E-mail addresses: jimin@dlut.edu.cn, wangmin@dlut.edu.cn

PTC-DRM experiment：

The PTC-DRM reaction was carried out in a fixed-bed reactor with an inner diameter of 20 mm (Fig. S1). A 300 W xenon lamp was used as a concentrated solar simulator, and two long-wavelength pass filters (400 nm and 490 nm, Edmund Optics) were employed to study wavelength-dependent characteristics. The catalyst temperature reached 167 °C under 300 W irradiation without auxiliary heating (Fig. S2). A quartz reactor with a dedicated light window (upper section: 2 mm × 10 mm square quartz tube; lower section: 8 mm inner diameter circular quartz tube) was used, and a thermocouple in direct contact with the catalyst surface was connected to a temperature controller to maintain consistent temperatures under light and dark conditions.

Before the reaction, 0.06 g of catalyst was mixed with 0.2 g of quartz sand, reduced in H_2 at 700 °C for 1.5 h, and purged with N_2 to remove residual H_2. The preheating furnace was heated to 350 °C, and upon reaching a reaction temperature of 550 °C, N_2 flow was replaced with a gas mixture of 30 mL·min^{-1} CO_2 and 30 mL·min^{-1} CH_4. The exhaust gas composition was analyzed by gas chromatography. Thermal catalytic activity was evaluated at 550-700 °C with a gas hourly space velocity (GHSV) of 60000 mL·g^{-1}·h^{-1}. Stability tests were conducted at 650 °C under light and dark conditions. The conversion efficiencies of CH_4 and CO_2 and the H_2/CO ratio were calculated using the following formulas :

$$CH_4\ conversion\ (\%) = \frac{F_{CH_{4,in}} - F_{CH_{4,out}}}{F_{CH_{4,in}}} \times 100\% \quad (1)$$

$$CO_2\ conversion\ (\%) = \frac{F_{CO_{2,in}} - F_{CO_{2,out}}}{F_{CO_{2,in}}} \times 100\% \quad (2)$$

$$H_2/CO = \frac{F_{out} \cdot C_{out.H_2}}{F_{out} \cdot C_{out.CO}} \times 100\% \quad (3)$$

$$TOF(S^{-1}) = \frac{X \times M_{Ni}}{V_m \times m_{cat} \times m_{Ni} \times D_{Ni}} \times 100\% \quad (4)$$

$$D_{Ni}(\%) = \frac{2 \times H_2 uptake \times 10^{-6} \times M_{Ni} \times \delta}{m_{Ni}} \times 100\% \quad (5)$$

Where, F_{in} and F_{out} are the inlet and outlet volume flows of each component at standard temperature and pressure. M_{Ni} represents the molar mass of Ni (58.7 g·mol^{-1}), m_{Ni} is the actual Ni loading, V_m is the standard molar volume of gas (22.4 L·mol^{-1}), m_{cat} is the mass of the catalyst used for testing the TOF value (mg) and D_{Ni} represents the dispersion of the active metal Ni. X refers to the conversion rates of methane and carbon dioxide. H_2 uptake was quantitatively measured by H_2-TPD. δ is the chemical adsorption's chemical stoichiometric factor for the Ni/H mole ratio (1).

Kinetic studies

The kinetic experiment was conducted at temperatures ranging from 470 to 530°C, utilizing a GHSV of 144000 ml·g·cat^{-1}·h^{-1}. This approach was chosen to minimize the influence of external mass transfer limitations and facilitate achieving lower reactant conversion rates. The catalytic activities, as well as their corresponding TOF_{CH4} and TOF_{CO2} values, have been comprehensively summarized in Table S1. Furthermore, the linear relationship between ln(TOF) and 1/T is clearly depicted in Fig. 5(c)(d).The specific calculation process is carried out with reference to the research of Li et al. [1]

$$TOF(s^{-1}) = \frac{X_{CH_4} \times M_{Ni}}{V_m \times m_{cat} \times m_{Ni} \times D_{Ni}} \times 100\% \quad (1)$$

Where, M_{Ni} was the molar mass of Ni, m_{Ni} was the actual loading capacity of Ni, Vm was the standard molar volume, D_{Ni} was the active metal dispersion, and mcat was the mass of the catalyst used to test the TOF value.

$$r_{CH4} = k_{CH4} \cdot P_{CH4}^{\alpha} \cdot P_{CO2}^{\beta} \quad (2)$$

$$r_{CO2} = k_{CO2} \cdot P_{CH4}^{\alpha} \cdot P_{CO2}^{\beta} \quad (3)$$

Where r_{CH4} and r_{CO2} were the reaction rates for CH_4 and CO_2, k_{CH4} and k_{CO2} were the rate constants for CH_4 and CO_2, α and β were the order of the reactions for CH_4 and CO_2, respectively.

The Arrhenius equation could be used to express k_{CH4} and k_{CO2} as follows:

$$k_{CH4} = A_{CH4} \cdot e^{\frac{-E_{aCH4}}{RT}} \quad (4)$$

$$k_{CO2} = A_{CO2} \cdot e^{\frac{-E_{aCO2}}{RT}} \quad (5)$$

Where A_{CH4} and A_{CO2} were the preexponential factor for CH_4 and CO_2, E_{aCH4} and E_{aCO2} were the activation energy for CH_4 and CO_2 respectively.[1]

Alternatively, r_{CH4} and r_{CO2} can be estimated through a combination of experimental data and H_2-chemisorption measurements. In particular, the turnover frequencies (TOF) can serve as substitutes for r_{CH4} and r_{CO2}. According to the Arrhenius equation, Ln(TOF) = -Ea/RT + C, the slope of the linear relationship between Ln(TOF) and 1/T is proportional to the activation energy divided by the gas constant (R). This analysis allows us to determine the activation energies for methane (E_{aCH4}) and carbon dioxide (E_{aCO2}) for Ni-Al, Ni-Ce-Al, Ni-Y-Al and Ni-Pr-Al.

A method for determining the carbon gasification rate by using CO_2 oxidation of deposited carbon over spent catalysts was used as follows, which was based on a modified Wigner–Polanyi equation (often used to generate kinetic data for TPD process).[2] As only small amount of surface carbon was identified on spent catalysts, and most of which can be gasified by CO_2 via reverse Boudouard reaction (reaction 6) to CO, by assuming that the reverse reaction and re-adsorption are negligible, the following gasification kinetic law (Eq. (7)) applies to the CO_2 surface gasification process.[3] These conditions are satisfied under our CO_2-excessive CO_2-TPO conditions operating under the high flow rate of carrier gas (He, 30 ml min^{-1}), and first order reaction to surface carbon concentration was identified before.[1]

$$C^* + CO_2 = 2CO^* + {}^* \quad (6)$$

$$r = -\frac{d\theta^*}{dt} = A\theta^* exp[-\frac{E_a}{RT}] \times P_{CO_2}^n \quad (7)$$

Where A is the pre-exponential factor, θ* is the surface carbon coverage, E_a is the activation energy and n is the reaction order with respect to CO_2 partial pressure. R and T are the universal gas constant and temperature, respectively. To determine the kinetic parameters, A, n and E_a need to be identified by regression. All samples were outgassed to 120 °C to remove surface contaminants during post-tests handlings under N_2 for 1 h, such as water. In the first series experiments, we used a tiny amount of spent catalysts (typically 10 mg) and a pure flow of CO_2, in order that the concentration variation of CO_2 can be deemed as constant. The samples placed at the bottom of the Ushaped quartz tube were investigated by heating the samples from 30 °C to 800 °C in CO_2 (100 vol.%) flow (30 ml min^{-1}) at heating rates of 5, 7.10, 15 °C min^{-1}, respectively. The CO_2 consumption was monitored by a TCD. Under such circumstances, a pseudo zeroth kinetic order for P_{CO2} applies, and E_a could therefore be measured by changing ramp of heating for CO_2-TPO,

$$r = -\frac{d\theta^*}{dt} = A\theta^* exp[-\frac{E_a}{RT}] \times P_{CO_2}^n = AP_{CO_2}^n \theta^* exp[-\frac{E_a}{RT}] \quad (8)$$

A$P_{CO_2}^n$can be regarded as an invariable, for the exceedingly high partial pressure and small consumption.

During the TPO analysis, the temperature is increased linearly by:

$$T_t = T_0 + \beta t \quad (9)$$

Where = β dT/dt and T_0 is the initial temperature. Thus:

$$-\frac{d\theta^*}{dT}\beta = AP_{CO_2}^n \theta^* exp[-\frac{E_a}{RT}] \quad (10)$$

If TM is the maximum temperature of a given TPO spectrum, then:

$$\frac{d}{dT}[\theta^* (\frac{AP_{CO_2}^n}{RT}) exp(\frac{E_a}{RT})] = 0 \quad (11)$$

$$2\ln T_M - ln\beta = \frac{E_a}{RT_M} + \ln(\frac{E_a}{AP_{CO_2}^n R}) \quad (12)$$

$2\ln T_M - \ln\beta$ vs. $1/T_M$ curve can be used to deduce Ea from the slope.

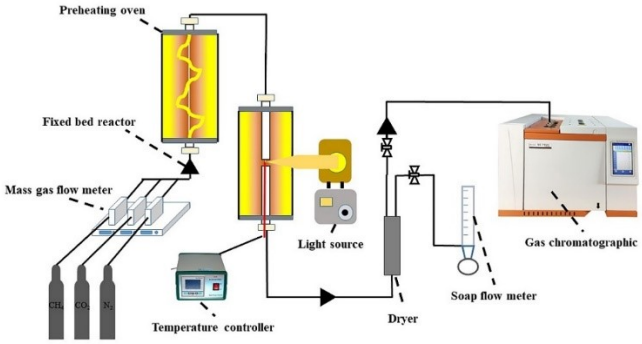

Fig. S1 Diagram of experimental device.

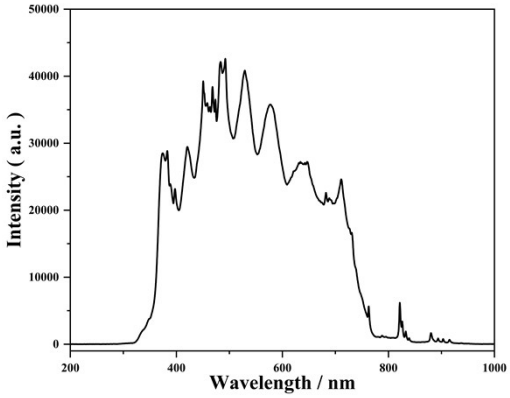

Fig. S2 Spectrum of 300 W xenon light source intensity for PTC reaction.

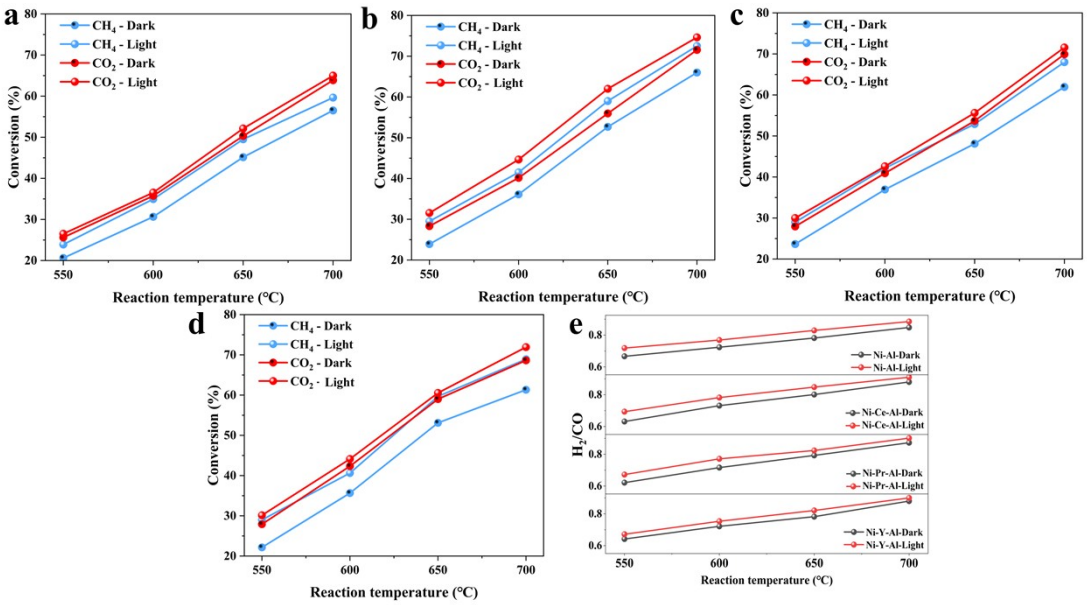

Fig. S3 PTC-DRM test of the catalysts (a) Ni-Al, (b) Ni-Ce-Al, (c) Ni-Pr-Al and (d) Ni-Y-Al catalysts, (e) H_2/CO.(Reaction conditions:WHSV=60000 mL·g^{-1}·h^{-1}, CH_4 / CO_2=1 / 1)

104 **Table S1** Comparison of catalyst performance with data in the literature.

Entry	Sample	Operating temperature (OA); Actual temperature of catalyst (AT)	Reactor type	Conditions	Production rates of CO and H_2 (PCO and PH_2)	Ref
1	$10Ni/Al_2O_3$	OT = 550℃ AT = NR	Flow-type reactor	LA-251Xe lamp with a HA30 filter (UV-visible light of 300−800 nm, 1.07 W cm^{-2}); 50 mg sample; Total feed flow rate is 20.0 mL/min (CH_4/CO_2 = 1:1); atmospheric pressure	PCO ≈ 6.50 μmol min^{-1} PH_2 ≈ 6.25 μmol min^{-1}	4
2	Pt/black TiO_2	OT = 550℃ AT = NR	Flow-type reactor	AM 1.5 G Newport solar simulator (100 mW/cm^{-2}); 15 mg sample; CH_4/CO_2 mixture gas (CH_4/CO_2= 1.0; GHSV = 40000 mL/g_{cat}/h)	PCO = 39.5 μmol min^{-1} PH_2 = 17.75 μmol min^{-1}	5
3	MgO/Pt/Zn-CeO_2	OT = 600℃ AT = 600℃	Flow-type reactor	A concentrated solar simulator (1200 W); 5 mg sample; 10% CH_4 and 10% CO_2; Total feed flow rate is 14 mL/min (CH_4/CO_2 = 1:1); 1.01 × 105 Pa	PCO = 43 μmol min^{-1} PH_2 = 29.7 μmol min^{-1}	6
4	Pt-Si-CeO_2	OT = 600℃ AT = 600℃	Flow-type reactor	A custom-made solar simulator (250–800 nm, 1775 mWcm^{-2}); 10 mg sample; Total feed flow rate is 14 mL/min (CH_4/CO_2 = 1:1)	PCO = 25.66 μmol min^{-1} PH_2 = 15 μmol min^{-1}	7
5	Ni-Ce-Al	OT = 650℃ AT = 650℃	Flow-type reactor	300 W Xe-lamp; 60 mg sample; Total feed flow rate is 60.0 mL/min (CH_4/CO_2 = 1:1); atmospheric pressure	PCO = 26.4 μmol min^{-1} PH_2 = 22.4 μmol min^{-1}	This work

105

Table S2. TOF_{CH4} and TOF_{CO2} of Ni-Al, Ni-Ce-Al, Ni-Pr-Al and Ni-Y-Al catalysts

Temperature (°C)			470	490	510	530
Ni-Al	Dark	$TOF_{CH4}(s^{-1})$	0.2077	0.2601	0.3219	0.3997
			(4.91%)[a]	(6.15%)[b]	(7.61%)	(9.45%)
		$TOF_{CO2}(s^{-1})$	0.3011	0.3565	0.4331	0.5223
			(7.12%)	(8.43%)	(10.24%)	(12.35%)
	Light	$TOF_{CH4}(s^{-1})$	0.2939	0.3578	0.4272	0.5143
			(6.95%)	(8.46%)	(10.10%)	(12.16%)
		$TOF_{CO2}(s^{-1})$	0.3176	0.3828	0.4542	0.5443
			(7.51%)	(9.05%)	(10.74%)	(12.87%)
Ni-Ce-Al	Dark	$TOF_{CH4}(s^{-1})$	0.2073	0.2424	0.3170	0.3751
			(6.25%)	(7.31%)	(9.56%)	(11.31%)
		$TOF_{CO2}(s^{-1})$	0.2723	0.3290	0.3983	0.4616
			(8.21%)	(9.92%)	(12.01%)	(13.92%)
	Light	$TOF_{CH4}(s^{-1})$	0.2905	0.3618	0.3979	0.4862
			(8.76%)	(10.91%)	(12.00%)	(14.66%)
		$TOF_{CO2}(s^{-1})$	0.3403	0.4092	0.4752	0.5359
			(10.26%)	(12.34%)	(14.33%)	(16.16%)
Ni-Pr-Al	Dark	$TOF_{CH4}(s^{-1})$	0.1207	0.1526	0.1801	0.2273
			(5.30%)	(6.70%)	(7.91%)	(9.98%)
		$TOF_{CO2}(s^{-1})$	0.1690	0.2022	0.2455	0.2959
			(7.42%)	(8.88%)	(10.78%)	(12.99%)
	Light	$TOF_{CH4}(s^{-1})$	0.1626	0.2034	0.2451	0.2847
			(7.14%)	(8.93%)	(10.76%)	(12.50%)
		$TOF_{CO2}(s^{-1})$	0.1781	0.2132	0.2505	0.3106
			(7.82%)	(9.36%)	(11.00%)	(13.64%)
Ni-Y-Al	Dark	$TOF_{CH4}(s^{-1})$	0.1614	0.1880	0.2450	0.2912
			(6.01%)	(7.00%)	(9.12%)	(10.84%)
		$TOF_{CO2}(s^{-1})$	0.2165	0.2595	0.3140	0.3675
			(8.06%)	(9.66%)	(11.69%)	(13.68%)
	Light	$TOF_{CH4}(s^{-1})$	0.2219	0.2595	0.3267	0.3788
			(8.26%)	(9.66%)	(12.16%)	(14.10%)
		$TOF_{CO2}(s^{-1})$	0.2418	0.2797	0.3441	0.3979
			(9.00%)	(10.41%)	(12.81%)	(14.81%)

[a] CH_4 conversion at different temperatures

[b] CO_2 conversion at different temperatures

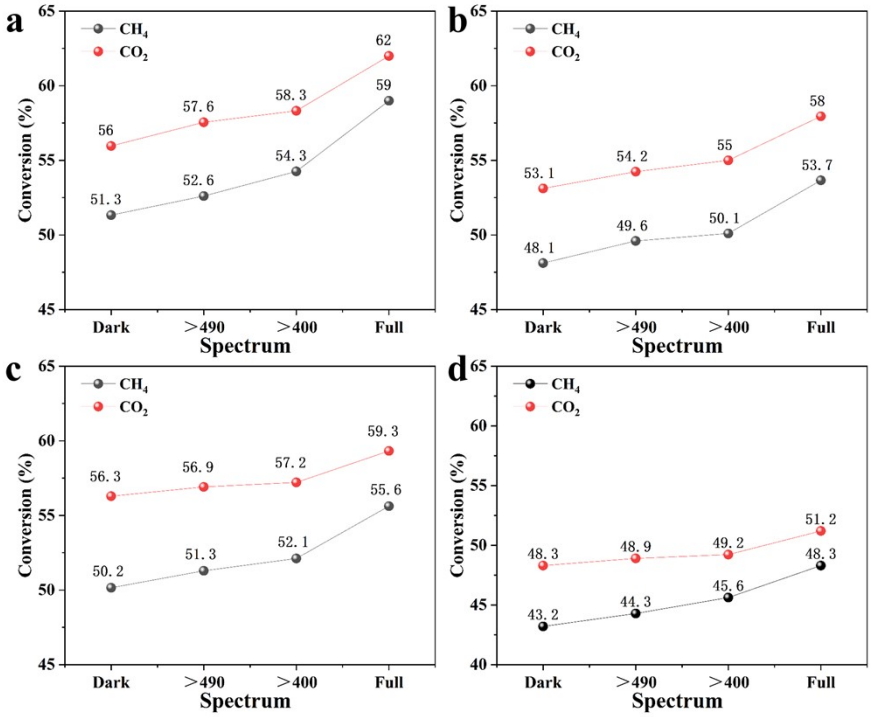

Fig. S4 Effect of different wavelengths of light source at 650 °C on the catalytic performance of (a) Ni-Ce-Al, (b) Ni-Pr-Al, (c) Ni-Y-Al and (d) Ni-Al (Reaction conditions:WHSV=60000 mL·g^{-1}·h^{-1}, CH_4 / CO_2 = 1 / 1)

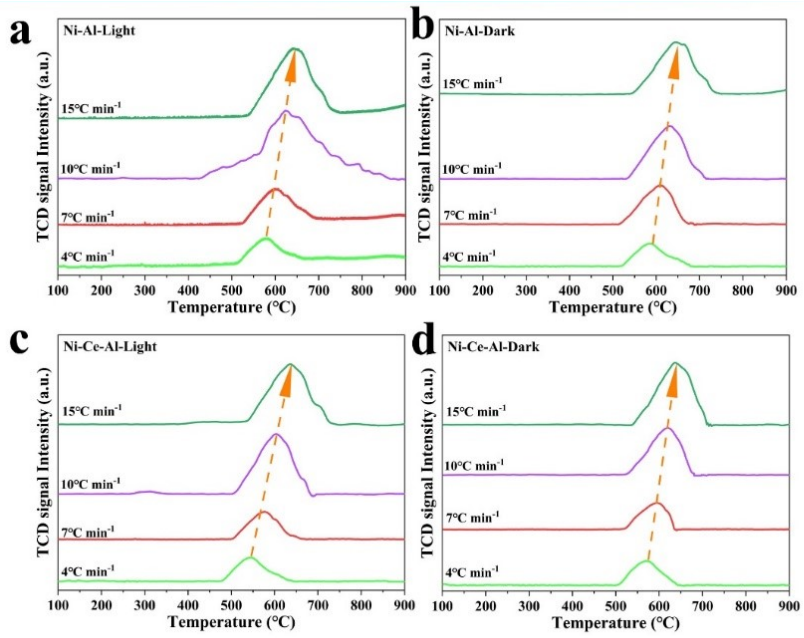

Fig. S5 CO_2-TPO patterns for Ni-Al and Ni-Ce-Al with manipulated rates of 4, 7, 10, 15 °C min^{-1} from 100 °C to 900 °C in CO_2 (100 vol.%) flow (30ml min^{-1})

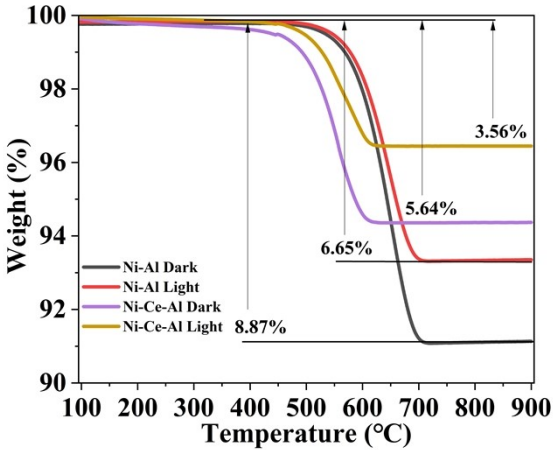

Fig. S6 Thermogravimetric curves of Ni-Ce-Al, and Ni-Al catalysts after thermal catalytic and photothermal catalytic reactions.

References

1 Li B, Yuan X, Li B, Wang X. Fuel. **2021**, 301, 121027.

2 H. Zhou, T. Zhang, Z. Sui, Y.-A. Zhu, C. Han, K. Zhu, X. Zhou, Appl. Catal. B-Environ. **2018**, 233, 143-159.

3 T. Osaki, Catal. Lett. **2015**, 145, 1931-1940.

4 H. Liu, T.D. Dao, L. Liu, X. Meng, T. Nagao, J. Ye, Appl. Catal. B-Environ. 2017, **209**, 183-189.

5 B. Han, W. Wei, L. Chang, P. Cheng, Y.H. Hu, ACS Catal. 2015, **6**, 494-497.

6 F. Pan, X. Xiang, Z. Du, E. Sarnello, T. Li, Y. Li, Appl. Catal. B-Environ. 2020, **260**, 118189.

7 F. Pan, X. Xiang, W. Deng, H. Zhao, X. Feng, Y. Li, ChemCatChem 2018, 10, 940-945.